9
Upland Erosion Modeling

Pierre Y. Julien, Mark L. Velleux, Un Ji, and Jaehoon Kim

Contents

Abstract Significant advances in upland erosion modeling have been achieved in the past decade. The TREX (Two-dimensional Runoff, Erosion, and Export) watershed model has been developed at Colorado State University for the simulation of surface runoff from spatially and temporally distributed rainstorms on watersheds. The model has been applied in several countries with different climatic conditions. TREX can calculate surface infiltration, surface runoff, sediment transport, and the partition of metals in dissolved, adsorbed, and particulate form. The focus of this chapter is on the calculation of surface flows and total suspended solids at the watershed scale. The chapter is comprised of three parts: (a) a description of the main processes and governing equations, (b) a description of the model components and algorithms, and (c) an application example on a large watershed. The application example for Naesung Stream in South Korea provides powerful visual evidence of upland erosion processes at the watershed scale during large rainstorms (300 mm of rainfall). Model calibration was successful and overall model performance is acceptable. Hydrologic simulation results were in good to very good agreement with measured flow volume, peak flow, and time to peak at the watershed outlet as well as several stations within the watershed. Sediment transport simulation results were also in reasonable agreement with the measured suspended solids concentration.

From: *Handbook of Environmental Engineering, Volume 15: Modern Water Resources Engineering*
Edited by: L.K. Wang and C.T. Yang, DOI 10.1007/978-1-62703-595-8_9,

Key Words Upland erosion • Distributed model • Extreme events • Sediment transport.

LIST OF SYMBOLS

a	Experimentally determined constant for flocculation
A	USLE (annual) average soil loss (tons/acre/year) [M L^{-2} T^{-1}]
A_c	Cross-sectional area of flow [L^2]
B_e	Width of eroding surface in flow direction [L]
B_x, B_y	Flow width in the x- or y-direction [L]
$\hat{C}$	USLE soil cover factor [dimensionless]
C_s	Concentration of sediment particles in the water column [M L^{-3}]
C_{sb}	Concentration of sediment particles in the soil or sediment bed [M L^{-3}]
C_t	Concentration of entrained sediment at the transport capacity [M L^{-3}]
C_w	Concentration of entrained sediment particles by weight at the transport capacity [dimensionless]
d_f	Median floc diameter (μm) [L]
d_p	Particle diameter [L]
d_*	Dimensionless particle diameter [dimensionless]
f	Infiltration rate [L T^{-1}]
g	Gravitation acceleration [L T^{-2}]
G	Particle specific gravity [dimensionless]
h	Surface water depth (flow depth of water column) [L]
H_c	Capillary pressure (suction) head at the wetting front [L]
i_e	Excess precipitation rate [L T^{-1}]
i_n	Net (effective) rainfall rate at the surface [L T^{-1}]
J_c	Sediment transport capacity areal flux [M L^{-2} T^{-1}]
J_d	Deposition flux [M L^{-2} T^{-1}]
J_e	Erosion flux [M L^{-2} T^{-1}]
k	Empirically or theoretically derived coefficient for sediment transport capacity [M L^{-1} T^{-1}]
$\hat{K}$	USLE soil erodibility factor [dimensionless]
K_h	Effective hydraulic conductivity [L T^{-1}]
LS	Slope length-gradient factor normalized to a field with a standard length of 23.2 m (76.2 ft) and a slope of 9 % [dimensionless]
m	Experimentally determined constant for flocculation
n	Manning roughness coefficient [T $L^{-1/3}$]
P_c	Wetted perimeter of channel flow [L]
$\hat{P}$	USLE soil management practice factor [dimensionless]
P_{dep}	Probability of deposition [dimensionless]
q	Unit flow rate of water $= v_a\, h$ [L^2 T^{-1}]
q_c	Critical unit flow for erosion (for the aggregate soil matrix) [L^2 T^{-1}]
q_l	Lateral unit flow from overland plane to channel (floodplain) [L^2 T^{-1}]

q_p	Peak runoff rate (m^3/s) [$L^3\ T^{-1}$]
q_s	Total sediment transport capacity (kg/m s) [$M\ L^{-1}\ T^{-1}$]
q_x, q_y	Unit discharge in the x- or y-direction $= Q_x/B_x$, Q_y/B_y [$L^2\ T^{-1}$]
Q	Total discharge [$L^3\ T^{-1}$]
Q_v	Storm runoff volume (m^3) [L^3]
Q_x, Q_y	Flow in the x- or y-direction [$L^3\ T^{-1}$]
R	Rainfall erosivity factor [dimensionless]
R_h	Hydraulic radius of flow $= A_c/P$ [L]
S_f	Friction slope [dimensionless]
S_{fx}, S_{fy}	Friction slope (energy grade line) in the x- or y-direction [dimensionless]
S_{0x}, S_{0y}	Ground surface slope in the x- or y-direction [dimensionless]
t	Time [T]
v_a	Advective (flow) velocity (in the x- or y-direction) [$L\ T^{-1}$]
v_c	Critical velocity for soil or sediment erosion [$L\ T^{-1}$]
v_r	Resuspension (erosion) velocity [$L\ T^{-1}$]
v_s	Quiescent settling velocity [$L\ T^{-1}$]
v_{se}	Effective settling (deposition) velocity [$L\ T^{-1}$]
v_{sf}	Floc settling velocity (cm/s) [$L\ T^{-1}$]
Y_e	MUSLE sediment yield from an individual storm [M]
α_c	Empirical soil erosion coefficient $= 11.8$
α_x, α_y	Resistance coefficient for flow in the x- or y-direction [$L^{1/3}\ T^{-1}$]
β	Resistance exponent $= 5/3$ (assuming Manning resistance) [dimensionless]
β_e	Empirical soil erosion exponent $= 0.56$ [dimensionless]
β_s	Empirically or theoretically derived exponent for discharge [dimensionless]
γ_s	Empirical or theoretically derived exponent for local energy gradient [dimensionless]
θ	Initial soil moisture deficit [dimensionless]
ρ_b	Bulk density of sediments [$M\ L^{-3}$]
ν	Kinematic viscosity of water [$L^2\ T^{-1}$]

1. UPLAND EROSION PROCESSES

A brief review of upland hydrologic and sediment transport processes is first presented. The main hydrologic processes include: (a) rainfall precipitation and interception, (b) snowmelt, (c) infiltration and transmission losses, (d) depression storage, and (e) overland and channel flow. Rainfall precipitation is usually determined from a network of point rain gage measurements or remotely sensed from radars. Rain gage measurements are usually more reliable, but radars usually provide a better spatial distribution of the rainfall patterns which may change with time as storms move through the watershed area. Snowmelt can be determined from radiative energy balance formulations or from empirical formulas based on daily temperature.

Infiltration is the downward transport of water from the surface to the subsurface. The rate at which infiltration occurs may be affected by several factors including hydraulic

conductivity, capillary action, and gravity (percolation) as the soil matrix reaches saturation. Many relationships [1–4] have been used to describe infiltration. The Green and Ampt relationship is often used because of its ease of application. For single storm events, the recovery of infiltration capacity by evapotranspiration and percolation can be neglected. Similarly, the loss to evaporation or other processes can also be neglected for single storm events.

Water may be stored in depressions on the land surface as small, discontinuous surface pools. In effect, the depression storage depth represents a threshold limiting the occurrence of overland flow. Note that water in depression storage is still subject to infiltration and evaporation.

1.1. *Surface Runoff*

Overland flow occurs when the water depth on the overland plane exceeds the depression storage threshold. Overland flow is governed by conservation of mass (continuity) and conservation of momentum. The two-dimensional (vertically integrated) continuity equation for gradually varied flow [5, 6] over a plane in rectangular (x, y) coordinates is:

$$\frac{\partial h}{\partial t} + \frac{\partial q_x}{\partial x} + \frac{\partial q_y}{\partial y} = i_\mathrm{n} - f = i_\mathrm{e} \tag{9.1}$$

where h = surface water depth [L]
q_x, q_y = unit discharge in the x- or y-direction = Q_x/B_x, Q_y/B_y [$\mathrm{L^2\ T^{-1}}$]
Q_x, Q_y = flow in the x- or y-direction [$\mathrm{L^3\ T^{-1}}$]
B_x, B_y = flow width in the x- or y-direction [L]
i_n = net (effective) rainfall rate at the surface [$\mathrm{L\ T^{-1}}$]
f = infiltration rate [$\mathrm{L\ T^{-1}}$]
i_e = excess precipitation rate [$\mathrm{L\ T^{-1}}$]

Momentum equations for the x- and y-directions may be derived by relating the net forces per unit mass to flow acceleration [5, 6]. In full form, with all terms retained, these equations can be expressed in dimensionless form as the friction slope and are known as the Saint-Venant equations. The full dynamic wave formulation of the Saint-Venant equations can normally be simplified to the diffusive wave approximation (of the friction slope) for the x- and y-directions:

$$S_{\mathrm{f}x} = S_{0x} - \frac{\partial h}{\partial x} \tag{9.2}$$

$$S_{\mathrm{f}y} = S_{0y} - \frac{\partial h}{\partial y} \tag{9.3}$$

where
$S_{\mathrm{f}x}$, $S_{\mathrm{f}y}$ = friction slope (energy grade line) in the x- or y-direction [dimensionless]
S_{0x}, S_{0y} = ground surface slope in the x- or y-direction [dimensionless]

To solve the overland flow equations for continuity and momentum, the hydraulic variables must be defined in terms of a depth-discharge relationship to describe flow resistance. Assuming that flow is turbulent and resistance can be described using the Manning formulation (in S.I. units), the depth-discharge relationships are:

$$q_x = \alpha_x h^{\beta} \tag{9.4}$$

$$q_y = \alpha_y h^{\beta} \tag{9.5}$$

$$\alpha_x = \frac{{S_{fx}}^{1/2}}{n} \tag{9.6}$$

$$\alpha_y = \frac{{S_{fy}}^{1/2}}{n} \tag{9.7}$$

where
α_x, α_y = resistance coefficient for flow in the x- or y-direction [$L^{1/3}\ T^{-1}$]
β = resistance exponent = 5/3 [dimensionless]
n = Manning roughness coefficient [$T\ L^{-1/3}$]

Similarly, channel flow can occur when the water depth in the channel exceeds the dead storage threshold. Channel flow is also governed by conservation of mass (continuity) and conservation of momentum. At the watershed scale, it is convenient to represent channel flows in a watershed as one-dimensional (along the channel in the down-gradient direction). The one-dimensional (laterally and vertically integrated) continuity equation for gradually varied flow along a channel is

$$\frac{\partial A_c}{\partial t} + \frac{\partial Q}{\partial x} = q_l \tag{9.8}$$

where
A_c = cross-sectional area of flow [L^2]
Q = total discharge [$L^3\ T^{-1}$]
q_l = lateral unit flow (into or out of the channel) [$L^2\ T^{-1}$]

Based on the momentum equation for the down-gradient direction and again neglecting terms for local and convective acceleration, the diffusive wave approximation may be used for the friction slope (see (9.2)). To solve the channel flow equations for continuity and momentum [5, 6], the Manning relationship may be used to describe flow resistance:

$$Q = \frac{1}{n} A_c {R_h}^{2/3} {S_f}^{1/2} \tag{9.9}$$

where
R_h = hydraulic radius of flow = A_c/P_c [L]
P_c = wetted perimeter of channel flow [L]

1.2. Upland Erosion

Erosion is the entrainment (gain) of material from a bottom boundary into surface flow by the action of water. The erosion flux may be expressed as a mass rate of particle removal from the boundary over time and the concentration (bulk density) of particles at the boundary:

$$J_e = v_r C_{sb} \tag{9.10}$$

where
J_e = erosion flux [M L^{-2} T^{-1}]
v_r = resuspension (erosion) velocity [L T^{-1}]
C_{sb} = concentration of sediment at the bottom boundary (in the bed) [M L^{-3}]

Entrained material may be transported as either bedload or suspended load. However, for overland sheet and rill flows, bedload transport by rolling and sliding may predominate as the occurrence of saltation and full suspension may be limited [7]. Entrainment rates may be estimated from site-specific erosion rate studies or, in general, from the difference between sediment transport capacity and advective fluxes:

$$v_r = \begin{cases} \dfrac{J_c - v_a C_s}{\rho_b} & \text{for} \quad J_c > v_a C_s \\ 0 & \text{for} \quad J_c \leq v_a C_s \end{cases} \tag{9.11}$$

where
v_r = resuspension (erosion) velocity [L T^{-1}]
J_c = sediment transport capacity areal flux [M L^{-2} T^{-1}]
v_a = advective (flow) velocity (in the x- or y-direction) [L T^{-1}]
C_s = concentration of sediment entrained in the flow [M L^{-3}]
ρ_b = bulk density of bed sediments [M L^{-3}]

In the overland plane, particles can be detached from the bulk soil matrix by raindrop (splash) impact and entrained into the flow by hydraulic action when the exerted shear stress exceeds the stress required to initiate particle motion [7, 8]. The overland erosion process is influenced by many factors including precipitation (rainfall) intensity and duration, runoff length, surface slope, soil characteristics, vegetative cover, exerted shear stress, and particle size. Raindrop impact may generally be neglected when flow depths are greater than three times the average raindrop diameter [6].

1.3. Soil Erosion Relationships

Extensive review of hillslope and watershed-scale soil erosion models is presented by [9, 10]. Soil erosion relationships range in complexity from simple empirical equations to physically based models that are applicable over different spatial and temporal scales. Common soil erosion relationships include the Universal Soil Loss Equation (USLE) and its variants. The USLE [11] is an empirical based on a large database of field plot measurements. It was developed to predict soil losses from agriculture and is designed to estimate long-term average annual soil loss associated with sheet and rill erosion using six factors that are associated with climate, soil, topography, vegetation, and land use management:

$$A = R\hat{K}\,LS\hat{C}\,\hat{P} \tag{9.12}$$

where
A = average annual soil loss due to sheet and rill erosion (tons/acre/year) [M L^{-2} T^{-1}]
R = rainfall erosivity factor [dimensionless]
$\hat{K}$ = soil erodibility factor (tons/acre) [dimensionless]
LS = slope length-gradient factor normalized to a field with a standard length of 23.2 m (76.2 ft) and a slope of 9 % [dimensionless]
$\hat{C}$ = cropping-management factor normalized to a tilled area that is continuously fallow [dimensionless]
$\hat{P}$ = conservation practice factor normalized to straight-row farming up and down the slope [dimensionless]

The Revised Universal Soil Loss Equation (RUSLE) and later versions of the RUSLE framework [12–14] have the same basic form as the original USLE but use extended methods to calculate how soil erosion factors are determined. In particular, a subfactor approach to determine crop management factors enables RUSLE to be applied to crops and management systems that were not examined in the original experiments used to develop the USLE. RUSLE is applicable to one-dimensional hillslopes that do not produce deposition as a result of changes in slope gradient. RUSLE2 [15] provides an approach that estimates erosion on a daily basis and accounts for deposition resulting from slope gradient changes on hillslopes.

The Modified Universal Soil Loss Equation (MUSLE) [16] estimates soil erosion loss (yield) for a single storm event by replacing the rainfall erosivity factor with a runoff energy factor determined by flow:

$$Y_e = \alpha_c \left(Q_v q_p\right)^{\beta_e} \hat{K}\,LS\hat{C}\,\hat{P} \tag{9.13}$$

where
Y_e = sediment yield from an individual storm (tons/acre) [M L^{-2}]
Q_v = storm runoff volume (m^3) [L^3]
q_p = peak runoff rate (m^3/s) [L^3 T^{-1}]

α_c = empirical soil erosion coefficient = 11.8
β_e = empirical soil erosion exponent = 0.56 [dimensionless]

More detailed review of the USLE family of soil erosion relationships is presented by [17].

1.4. Overland Sediment Transport Capacity Relationships

Building on the initial work of [7], Prosser and Rustomji [18] summarized relationships to describe the sediment transport capacity of overland flow. A generalized overland flow sediment transport capacity equation is

$$q_s = k\, q^{\beta_s} S_f^{\gamma_s} \tag{9.14}$$

where
q_s = total sediment transport capacity [M L^{-1} T^{-1}]
k = empirically or theoretically derived coefficient for sediment transport capacity [M L^{-1} T^{-1}]
q = unit flow (discharge) of water [L^2 T^{-1}]
β_s = empirically or theoretically derived exponent for discharge [dimensionless]
S_f = friction slope (local energy gradient) [dimensionless]
γ_s = empirical or theoretically derived exponent for local energy gradient [dimensionless]

The sediment transport capacity coefficient (k) represents the combined influence that rainfall intensity, overland flow, and landscape and particle characteristics such as soil erodibility, infiltration, surface roughness, and vegetative cover have on sediment transport. Extending the review of discharge (β_s) and local energy gradient (γ_s) exponent values presented by [7], more recent research by [18] concluded that values of $1.0 \leq \beta_s \leq 1.8$ and $0.9 \leq \gamma_s \leq 1.8$ are generally applicable for use in soil erosion modeling.

Julien [6, 19] recommends a modified form of the Kilinc and Richardson relationship [20] that includes soil erodibility, cover, and management practice terms from the Universal Soil Loss Equation (USLE) [21] to estimate the total overland sediment transport capacity (for both the x- and y-directions):

$$q_s = 1.542 \times 10^8 q^{2.035} S_f^{1.66} \hat{K}\, \hat{C}\, \hat{P} \tag{9.15}$$

$$J_c = \frac{q_s}{B_e} \tag{9.16}$$

where
q_s = total sediment transport capacity (kg/m s) [M L^{-1} T^{-1}]
q = unit flow rate of water = $v_a\, h$ [L^2 T^{-1}]
S_f = friction slope [dimensionless]
$\hat{K}$ = USLE soil erodibility factor [dimensionless]

$\hat{C}$ = USLE soil cover factor [dimensionless]
$\hat{P}$ = USLE soil management practice factor [dimensionless]
B_e = width of eroding surface in flow direction [L]

1.5. Channel Transport Capacity Relationships

In channels, sediment particles can be entrained into the flow when the exerted shear stress exceeds the stress required to initiate particle motion. For non-cohesive particles, the channel erosion process is influenced by factors such as particle size, particle density, and bed forms. For cohesive particles, the erosion process is significantly influenced by interparticle forces (such as surface charges that hold grains together and form cohesive bonds) and consolidation. Total (bed material) load transport capacity relationships account for the both bedload and suspended load components of sediment transport. Yang and Julien [19, 22] provide summaries of numerous total load transport relationships. The Engelund and Hansen relationship [23] is considered a reasonable estimator of the total load:

$$C_w = 0.05\left(\frac{G}{G-1}\right)\frac{v_a S_f}{\left[(G-1)g d_p\right]^{0.5}}\left[\frac{R_h S_f}{(G-1)d_p}\right]^{0.5} \tag{9.17}$$

$$J_c = \frac{v_a C_t}{A_c} \tag{9.18}$$

where
C_w = concentration of entrained sediment particles by weight at the transport capacity [dimensionless]
G = particle specific gravity [dimensionless]
v_a = advective (flow) velocity (in the down-gradient direction) [L T^{-1}]
S_f = friction slope [dimensionless]
R_h = hydraulic radius of flow [L]
g = gravitation acceleration [L T^{-2}]
d_p = particle diameter [L]
J_c = advection flux [M L^{-2} T^{-1}]
A_c = cross-sectional area of flow [L^2]
C_t = concentration of entrained sediment particles at the transport capacity = $10^6 G C_w/[G + (1 - G)C_w]$ (g/m^3) [M L^{-3}]

It is worth noting that one feature common to both (9.15) and (9.17) is that the implicit threshold for incipient motion is zero. This means that the transport capacity of any particle will always be greater than zero, regardless of particle size or the exerted shear stress, as long as the unit flow or flow velocity and friction slope are nonzero. This can lead to inconsistent results when erosion rates are computed from sediment transport capacities. The inferred erosion rate will almost always be greater than zero because the difference between the

transport capacity and advective flux will nearly always be greater than zero. Consequently, a nonzero erosion rate can be computed even when the exerted shear stress is far less than the incipient motion threshold for the material. To address this limitation, an incipient motion threshold can be added to the modified relationships [20, 23]:

$$q_s = 1.542 \times 10^8 (q - q_c)^{2.035} S_f^{1.66} \hat{K}\,\hat{C}\,\hat{P} \tag{9.19}$$

$$C_w = 0.05 \left(\frac{G}{G-1}\right) \frac{(v_a - v_c) S_f}{\left[(G-1) g d_p\right]^{0.5}} \left[\frac{R_h S_f}{(G-1) d_p}\right]^{0.5} \tag{9.20}$$

where
q_c = critical unit flow for erosion (for aggregate the soil matrix) = $v_c h$ [L^2 T^{-1}]
v_c = critical velocity for erosion [L T^{-1}]
h = surface water depth [L]

1.6. Deposition

Deposition is the sedimentation (loss) of material entrained in a flow to a bottom boundary by gravity. The deposition process is influenced by many factors including particle density, diameter and shape, and fluid turbulence. The deposition flux may be expressed as a mass rate of particle removal from the water column over time and the concentration of sediment particles that are entrained in the flow:

$$J_d = v_{se} C_s \tag{9.21}$$

where
J_d = deposition flux [M L^{-2} T^{-1}]
v_{se} = effective settling (deposition) velocity [L T^{-1}]
C_s = concentration of sediment particles in the flow [M L^{-3}]

Coarse particles (>62 μm) are typically inorganic and non-cohesive and generally have large settling velocities under quiescent conditions. Numerous empirical relationships to describe the non-cohesive particle settling velocities are available. Summaries of relationships and settling velocities are presented by [19, 22]. For non-cohesive (fine sand) particles with diameters from 62 to 500 μm, the settling velocity [24] can be computed as

$$v_s = \frac{\nu}{d_p} \left[\left(25 + 1.2 d_*^2\right)^{0.5} - 5\right]^{1.5} \tag{9.22}$$

$$d_* = d_p \left[\frac{(G-1) g}{\nu^2}\right]^{1/3} \tag{9.23}$$

where
v_s = quiescent settling velocity [L T^{-1}]
ν = kinematic viscosity of water [L^2 T^{-1}]
d_* = dimensionless particle diameter [dimensionless]
d_p = particle diameter [L]

Medium particles (10 μm < d_p < 62 μm) can vary in character. Inorganic particles may behave in a non-cohesive manner. In contrast, organic particles (potentially including particles with organic coatings) may behave in a cohesive manner. Fine particles (<10 μm) often behave in a cohesive manner. If behavior is largely non-cohesive, settling velocities may be estimated as described by Julien [19]. If the behavior is cohesive, flocculation may occur. Floc size and settling velocity depend on the conditions under which the floc was formed [25–27]. When flocculation occurs, settling velocities of cohesive particles can be approximated by relationship of the form [25]:

$$v_{sf} = a d_f^{\,m} \tag{9.24}$$

where
v_{sf} = floc settling velocity (cm/s) [L T^{-1}]
a = experimentally determined constant = 8.4×10^{-3}
d_f = median floc diameter (μm) [L]
m = experimentally determined constant = 0.024

However, depending on fluid shear, particle surface charge, and other conditions, fine particles may not flocculate. Under conditions that limit floc formation, fine particles can have very small, near zero settling velocities.

As a result of turbulence and other factors, not all particles settling through a column of flowing water will necessarily reach the sediment-water interface or be incorporated into the sediment bed [28]. Beuselinck [29] suggests that this process also occurs for the overland plane. As a result, effective settling velocities in flowing water can be much less than quiescent settling velocities. The effective settling velocity of a particle can be described as a reduction in the quiescent settling velocity by the probability of deposition [28, 30]:

$$v_{se} = P_{dep} v_s \tag{9.25}$$

where
v_{se} = effective settling velocity [L T^{-1}]
v_s = quiescent settling velocity [L T^{-1}]
P_{dep} = probability of deposition [dimensionless]

2. WATERSHED MODELING

A range of watershed modeling methods and frameworks exist. Methods include unit hydrograph/lumped parameter, advanced lumped parameter/semi-distributed, and fully distributed, physically based approaches. Singh [31] presents descriptions of numerous watershed models. Each approach has characteristic strengths and limitations, and there are trade-offs between the spatial and temporal detail used to represent physical processes and model performance. Although methods used differ, all model frameworks reviewed have the ability to simulate runoff. Some frameworks can simulate soil erosion. A few models can also simulate stream sediment transport (erosion and deposition) processes. Even fewer have the specialized capabilities to simulate chemical transport.

Key milestones in the development of fully distributed, physically based watershed models include CASC2D (and CASC2D-SED) [5, 32–35], GSSHA [36], the SHE series of models [37–40], and TREX [41, 42]. The starting point for TREX development was CASC2D. Like CASC2D, the TREX framework is an event-based model that simulates overland flow, surface soil erosion and deposition, stream flow, and sediment transport through streams. As part of the TREX development, hydrologic and sediment transport components of CASC2D were expanded to support chemical transport. A complete review of hydrologic, sediment transport (and chemical transport) processes to describe the physics behind the model is provided by [41] and [43]. Further descriptions of CASC2D and TREX follow.

2.1. *CASC2D*

CASC2D (including CASC2D-SED) is a fully distributed, physically based, event-oriented model that simulates rainfall, interception, infiltration, overland flow, channel flow, as well as sediment erosion and deposition [5, 32–35, 44]. For surface waters, flow routing is performed using the diffusive wave approximation and is two-dimensional overland and one-dimensional in channels. CASC2D does not include groundwater flow processes other than infiltration and Hortonian overland flow. However, it can be directly coupled with GIS-based site characterization data obtained from remote sensing sources.

CASC2D has been applied at a wide variety of spatial scales from large river basins (12,000 km^2) to moderate watersheds (560 km^2) [45] to small watersheds (20–30 km^2) [44]. Overland and channel erosion are computed using the modified form of the Kilinc-Richardson [20, 23, 33]. Up to three solids classes can be simulated [44]. Chemical transport and fate is not simulated. The CASC2D source code is publicly available.

2.2. *TREX*

A generalized conceptual framework for the TREX watershed model is presented in Fig. 9.1. TREX (Two-dimensional Runoff, Erosion, and Export) is a spatially distributed, physically based model that can be used to simulate precipitation, overland runoff, channel flow, soil erosion, stream sediment transport, and chemical transport and fate at the watershed scale [41–43, 46]. TREX combines surface hydrology and sediment transport features from

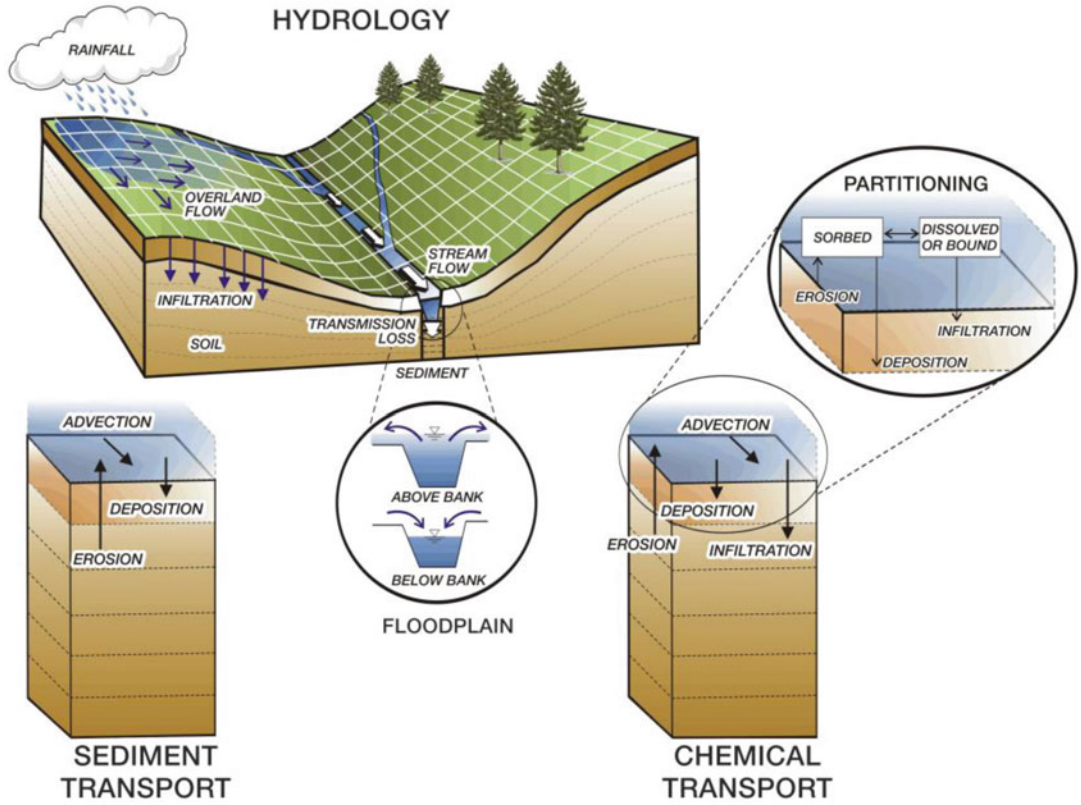

Fig. 9.1. TREX conceptual model framework.

the CASC2D watershed model [33, 35, 44] with chemical transport features from the WASP/IPX series of water quality models [47, 48].

Hydrologic processes simulated are (a) rainfall and snowfall (precipitation), interception, snowmelt, and surface storage; (b) infiltration and transmission loss; and (c) overland and channel flow. Model state variables are water depth in the overland plane and stream channels. Precipitation can be uniform or distributed in both time and space and can also be specified using several grid-based formats to facilitate radar precipitation data use. When spatially distributed precipitation is simulated, areal estimates are interpolated from point gage data using an inverse distance weighting approach. Interception and surface storage are simulated as equivalent depths. Infiltration and transmission loss rates are simulated using the Green and Ampt relationship [1]. Overland flow is two-dimensional and simulated using the diffusive wave approximation. Channel flow is one-dimensional and is also simulated using the diffusive wave approximation.

Sediment transport processes simulated are (a) advection-diffusion, (b) erosion and deposition, and (c) bed elevation adjustment. All processes are simulated in the overland plane and stream channels. Model state variables are solid concentrations in overland runoff, soil, stream flow, and stream bed sediment. Any number of particle size classes can be simulated.

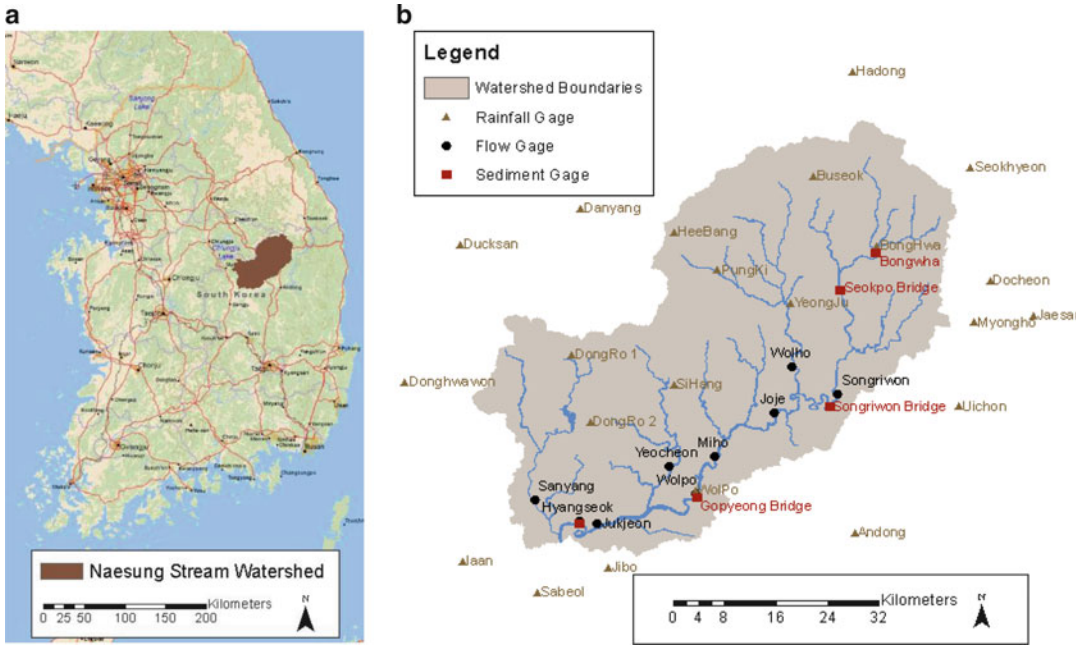

Fig. 9.2. Naesung Stream watershed and monitoring station locations. (**a**) Watershed location, Korea. (**b**) Rainfall, flow, and sediment monitoring stations.

In floodplain areas, water and transported constituents are transferred between the overland plane and channel network based on the difference in water surface elevations. Floodplain transfers are bidirectional. Water and transported sediments and chemicals move into stream channels by overland flow and can return to the overland plane when water levels in the stream exceed bank height. Similarly, materials can be moved from the sediment bed and can be delivered to the land surface by floodwaters. TREX source code, a user manual, reference material, and example files are freely available on the web.

3. WATERSHED MODEL APPLICATION

To demonstrate watershed modeling concepts, a case study application using TREX [41–43, 46] is presented. TREX was applied to the Naesung Stream watershed in Korea and was used to simulate hydrology and sediment transport. Soil erosion results from the model were used to identify erosion-prone areas.

3.1. Naesung Stream Site Description and Database

The Naesung Stream watershed is located in North Gyeongsang Province (Gyeongsangbuk-do), Korea, and drains an area of approximately 1,815 km^2 within the Nakdong River basin. Land surface elevations range from 54 to 1,420 m above mean sea

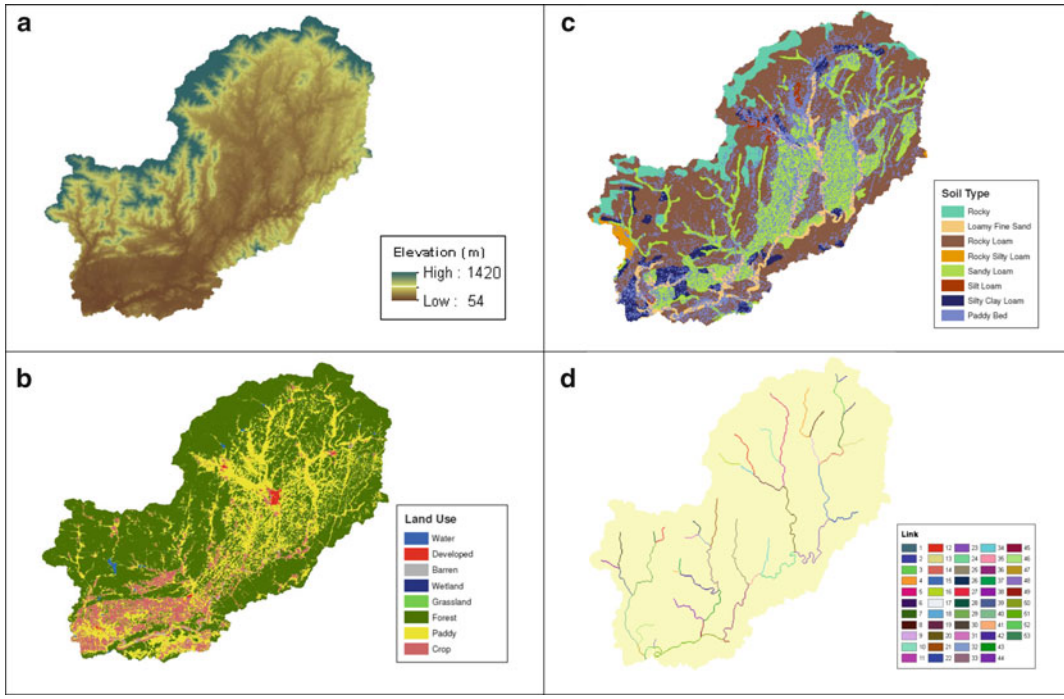

Fig. 9.3. Raster maps of (**a**) watershed elevations, (**b**) land uses, (**c**) soil types, and (**d**) the stream channel network (flow path links) at the 150-m scale.

level. The average channel slope of the stream is 0.009 m/m. The database for this watershed includes rainfall measurements reported at 22 monitoring stations, stream flows reported at 9 stations, suspended solids data at 11 stations, sediment discharges at 3 stations, and sediment yields estimated at 4 stations. Rainfall and flow data were reported on an hourly basis and were available for 2008 and 2009 as well as other periods. Maps displaying locations of the Naesung Stream watershed, stream network, and monitoring stations are presented in Fig. 9.2. Stations at Hyangseok, Miho, Wolho, and Yecheon provide stream flow measurements for subbasins within the watershed as well as near the watershed outlet. Stations at Hyangseok and Songriwon provide sediment discharge and yield estimates.

3.2. Naesung Stream Model Setup

The model requires data to describe watershed boundaries, the stream channel network, land surface elevations, soils, land use, and related information describing physical processes that control runoff and soil and sediment transport for any given rainfall event. All data were detailed in the Naesung Stream Watershed Data Collection [49] and Naesung Stream Watershed Bank Erosion [50] reports. Data included geographic information system (GIS) files for ArcGIS 9.3 [51], HEC-RAS hydraulic model files [52], as well as additional data such as stage-discharge relationships and sediment-discharge information.

Watershed land surface elevations were defined using digital elevation model (DEM) data. Soil types, land uses, and their spatial distributions were defined according to the associations and classes that occur within the watershed. DEM, soil, and land use data were provided at a 30-m resolution (1 arc s) and subsequently processed for model use at a 150-m grid scale (i.e., where each model cell is 150 m by 150 m). The 150-m grid scale was selected to improve model execution speed and reduce time required for simulations. Model grid scale affects accuracy of hydrology and sediment transport simulations [53]. Compared to higher resolution configurations (e.g., 30 or 90 m), use of a 150-m grid scale permits reasonable simulation of both hydrology and soil erosion. At the 150-m scale, the Naesung Stream watershed is comprised of 80,690 grid cells. The watershed DEM was also smoothed using a custom computer program created to reduce effects of anomalous elevations that resulted in deep pits in isolated areas of the watershed. Raster maps of watershed elevations, soil types, land uses, and the stream channel network at the 150-m scale are presented in Fig. 9.3.

Watershed boundaries and the stream channel network were delineated using TauDEM 4.0 [54]. For consistency with the Naesung Stream hydrography layer provided by Myongji University, the hydrography layer was converted from polygons to polylines in ArcGIS and then used to "burn" stream locations into the DEM prior to delineating the channel network. Using this approach, the stream network was defined as 53 links comprised of 2,135 nodes, yielding a total stream length of approximately 34.8 km and a drainage density of 0.2 km of stream length per square kilometer of watershed (0.2 km/km^2). Physical dimensions of the channel network (e.g., width, bank height, side slope) were determined from data contained in HEC-RAS geometry files for Naesung Stream.

Soil types and land use classes were defined based on major associations and classifications present in the watershed as described in the GIS files. In the "simple" GIS files, soil types and land use classes with similar characteristics were combined to simplify model setup. Soil types in the model were also modified to include rice paddy fields as a distinct soil type. Inclusion of paddy fields as a soil type was based on research indicating that paddy fields are often underlain by soil layers with lower hydraulic conductivities and higher clay contents [55].

Interception depths and depression storage depths for each land use class were assigned based on expected land use characteristics described in the literature [56–58]. For simplicity, depression storage depths for all land use classes other than paddy fields were set to zero. The paddy fields land use was specified to have 6 cm of depression storage to account for berms surrounding paddy fields [55]. Initial values for overland and channel flow resistance (Manning n) values were determined by land use and substrate [59, 60]. Manning n values for stream channels were regularized by assigning values into two classes: (1) rocky substrate streams (higher flow resistance) and (2) wider, sand bed streams (lower flow resistance). Final flow resistance values were determined by calibration.

Size distributions of particles comprising soils and sediments of the site vary with the strata from which they originate. Surface soils are typically dominated by silts with considerable fractions of sands and clays as well as gravel and other rock fragments. Bed sediments are

Table 9.1
Particle classes and properties

Particle class name	Representative size range (mm)	Effective diameter (d_p) (mm)	Specific gravity (G) (dimensionless)	Fall velocity (v_s) (m/s)	Critical shear stress for deposition (Pa)	Critical erosion velocity (v_c) (m/s)
Gravel-cobble	>16	32	2.65	0.678	26	1.39
Gravel	4–16	8	2.65	0.338	5.7	0.693
Sand	0.125–4	0.5	2.65	0.066	0.27	0.268
Silt/clay	>0.125	0.016	2.65	0.000167	0.065	0.022

dominated by sands and finer gravel. Overall, particles sizes range from coarse gravels and cobbles to silts and clays. There is a trade-off between the number of particle state variables (classes) used to represent solids and computational time needed for a simulation. Processing time increases as the number of state variables increases. Given the range of particle types present in the watershed, solids were simulated as four classes: (a) coarse gravels and coarser ("gravel-cobble"); (b) fine to coarse gravel ("gravel"); (c) coarse sands to fine gravels ("sands"); and (d) finer sands, silts, and smaller particles ("silt/clay").

Properties of each particle class, soils, and sediments were defined from values tabulated in the Myongji University database and supplemented by other literature as noted below. Properties specified include (a) effective particle diameter d_p, (b) particle specific gravity G, (c) particle fall velocity v_s, (d) soil and sediment porosity, (e) soil effective hydraulic conductivity K_h, (f) soil capillary suction head H_c, (g) soil erodibility $\hat{K}$, (h) erosion (incipient motion) thresholds for soil and sediment expressed as critical velocities v_c, and (i) grain size distributions for soils and sediments. Summaries of these properties, including physical characteristics of the channel network, are presented in Tables 9.1, 9.2, and 9.3.

Effective hydraulic conductivities and capillary suction heads were determined from soil types [61]. Final effective hydraulic conductivity values were determined by calibration. Soil erodibility $\hat{K}$, cover factor $\hat{C}$, and practice factor $\hat{P}$ values were estimated based on literature values summarized by [11, 19]. Soil effective porosities were estimated from maximum moisture content and field moisture content values for each soil type. Sediment porosity was assumed to be 0.5 uniformly in the riverbed.

In the overland plane, the soil column was defined as two layers with a total thickness of 15 cm (a 5-cm surface layer and a 10-cm subsurface layer). This total soil thickness is reasonable because a single event is not expected to completely denude the land surface of erodible, unconsolidated soils. In the channel network, the sediment bed was also defined as two layers with a total thickness of 20 cm (two 10-cm layers) underlain by non-erodible hardpan. This bed configuration was selected to represent conditions where particles from the streambed may have limited availability and that supply limited sediment transport occurs. Representation of the bed as two relatively thin layers over hardpan is reasonable because it is possible that large storm events could cause transport sufficient to erode all unconsolidated

Table 9.2
Soil classes and properties

Soil type	Critical erosion velocity v_c (m/s)	Effective porosity	K_h (m/s)	Initial soil moisture deficit (θ)	H_c (m)	$\hat{K}$ (tons/acre/year)	Soil grain size distribution			
							Gravel-cobble	Gravel	Sand	Silt/clay
Rocky	0.0071	0.44	8.35E-07	0.051–0.409	0.05	0.1	0.50	0.20	0.15	0.15
Loamy fine sand	0.0278	0.40	1.66E-07	0.047–0.387	0.061	0.44	0.00	0.05	0.75	0.20
Rocky loam	0.0118	0.43	4.18E-07	0.035–0.400	0.069	0.1	0.05	0.15	0.30	0.50
Rocky silty loam	0.0120	0.49	6.05E-08	0.037–0.371	0.137	0.16	0.10	0.15	0.15	0.60
Sandy loam	0.0238	0.41	3.33E-09	0.033–0.363	0.11	0.27	0.00	0.00	0.55	0.45
Silt loam	0.0339	0.49	1.89E-08	0.031–0.351	0.167	0.48	0.00	0.00	0.25	0.75
Silty clay loam	0.0244	0.43	5.55E-09	0.001–0.231	0.273	0.37	0.00	0.00	0.15	0.85
Paddy field	0.0244	0.43	4.68E-09	0.000	0.000	0.37	0.00	0.00	0.15	0.85

Notes: Lower soil moisture deficit values represent wet initial conditions for July 2008 and larger values represent drier conditions for July 2009.

Table 9.3
Land use classes and properties

Land use	Manning n	Interception depth (mm)	$\hat{C}$	$\hat{P}$
Wetland	0.100	0.00	0.000	1.00
Water	0.050	0.00	0.000	1.00
Developed	0.010	0.10	0.008	1.00
Barren	0.200	0.00	0.050	1.00
Grassland	0.300	1.00	0.013	1.00
Forest	0.400	2.00	0.002	1.00
Paddy	0.500	1.00	0.050	1.00
Crop	0.300	1.00	0.013	1.00

material from the bed in some locations. However, the maximum depth of bed scour (degradation) that can occur will be limited by the total thickness of bed sediment at the start of the simulation (i.e., 20 cm for this model setup).

It should be noted that several parameters summarized in Tables 9.1, 9.2, and 9.3 were subject to calibration (e.g., effective hydraulic conductivity, Manning n, soil moisture deficit). Values reported in these tables represent model setup from calibration to the July 24–26, 2008, and July 8–10, 2009, storm events. Model initial conditions that must be specified include baseflow and initial water depths, initial soil moisture deficit, depth of infiltrated water (soil moisture conditions), and suspended solids concentrations for each particle class. Soil moisture conditions were estimated based on review of rainfall records preceding the July 2008 and July 2009 storms. Conditions preceding the July 2008 storm were relatively wet as there was appreciable rain (i.e., more than 100 mm) in the days before the event. Conditions preceding the July 2009 storm were relatively dry as there was little rain (i.e., less than 10 mm) before the event. Soil moisture deficit values were refined by calibration. For simplicity, the initial depth of infiltrated water was assumed to be zero. Initial water depths on the overland plain were assumed to be zero except for rice paddy areas. For rice paddies, the initial water depth was assumed to be 3 cm for the July 2008 storm and 1 cm for the July 2009 storm. Initial water depths for paddy fields were refined by calibration. Initial suspended solids concentrations for the "silt/clay" particle class ranged from 1 g/m^3 (mg/L) to 10 g/m^3 and were zero for the remaining three particle classes.

Baseflow (i.e., stream flow for periods preceding storm events) was estimated by reviewing flow records at monitoring gages throughout the watershed. Flow conditions for the July 24–26, 2008, and July 8–10, 2009, storms appeared to be similar, so the same values were used for both events. The channel network includes 21 headwater branches (i.e., branches that are upstream of all other portions of the channel network). Baseflow was represented as a flow point source to the head of each headwater link in the channel network. Baseflow at Hyangseok was estimated to be 40 m^3/s based on flow monitoring data at Hyangseok.

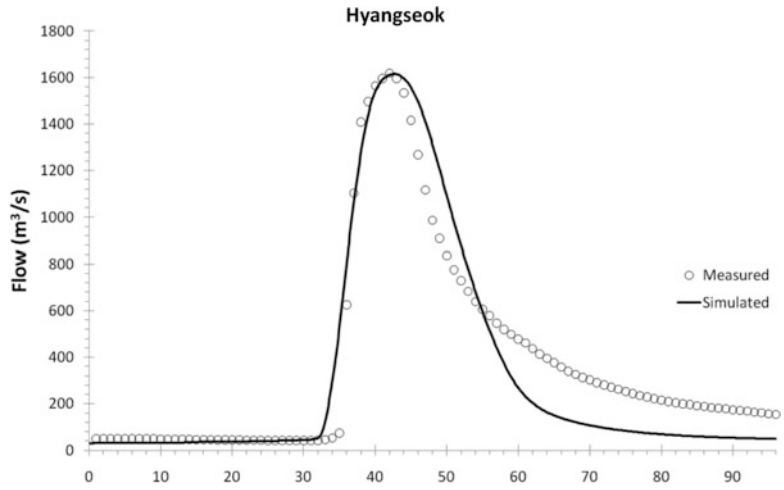

Fig. 9.4. Simulated and measured flows at Hyangseok: July 24–26, 2008, storm.

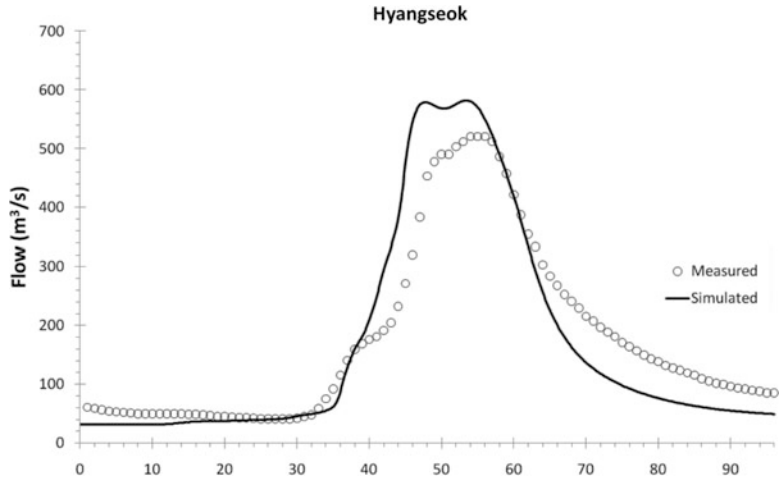

Fig. 9.5. Simulated and measured flows at Hyangseok: July 08–10, 2009, storm.

3.3. Model Calibration Results

3.3.1. Hydrology

The watershed model was calibrated by simulating rainfall, runoff, and sediment transport for two storms: (a) July 24–26, 2008, and (b) July 8–10, 2009. Rainfall for these events was defined by hourly measurements at 22 gages across the watershed. All simulations were 96 h in duration and included each storm's rainfall period (up to 48 h) and an additional 48 h to allow simulation of the recession limb of the hydrograph and return to baseflow conditions. As part of calibration, model parameters were iteratively varied until simulation results were in rough agreement with measured flows and sediment concentrations. Agreement between model results and measurements was assessed by graphical and statistical comparisons.

The hydrologic calibration was performed by varying the following parameters: effective hydraulic conductivity K_h, channel and overland flow resistance (Manning n), and initial soil moisture deficit θ. Effective hydraulic conductivity affects the total volume of runoff generated. Flow resistance influences the timing and magnitude of flow. Soil moisture conditions also affect runoff volume and the timing of flow through the system. As part of hydrologic calibration efforts, 12–18 individual model simulations were completed for each storm.

Calibrated hydrologic simulation results and measurements for the July 2008 and July 2009 storms are presented in Figs. 9.4 and 9.5 respectively. Statistical summaries comparing simulated and measured values for total flow volume, peak flow, and time to peak flow metrics are presented in Table 9.4. Statistical analyses include relative percent difference (RPD), Nash-Sutcliffe efficiency coefficient (NSEC), and root mean square error (RMSE). Model performance was generally good.

3.3.2. Sediment

Calibrated sediment transport simulation results and measurements for the July 2008 and July 2009 storms are presented as functions of flow in Figs. 9.6 and 9.7. Simulated and estimated values are presented for the Hyangseok station. Estimated values presented on these graphs represent values estimated from flow using reported sediment-discharge relationships at these stations. Tabular summaries comparing simulated, measured, and estimated values for suspended solids concentration and sediment yield rates are presented in Tables 9.5 and 9.6, respectively.

Simulated suspended solids concentrations are roughly within a factor of 2 to 3 of values estimated from flow and sediment-discharge relationships at Hyangseok. However, simulated suspended solids concentrations appear to be much smaller than estimated concentrations across the ranges of flows at Songriwon. Some of the differences between simulated values and concentrations estimated from sediment-discharge relationships may be attributable to uncertainty introduced by extrapolating discharge relationships beyond the flow ranges for which they were developed. Some differences between simulated and estimated concentrations may also be attributable to hydrologic model overestimation and underestimation errors at Songriwon as well as Hyangseok.

In Table 9.6, reported sediment yields and estimated yields represent values calculated using flow and sediment-discharge relationships for each station and normalized by drainage area. Similarly, simulated sediment yields were calculated using simulated flow and simulated suspended solids concentrations and normalized by drainage area. As a broad generality, simulated sediment yields are within the range of reported and estimated yields. However, differences between reported and estimated sediment yield values are large, suggesting large uncertainties in the underlying database used for model development. Given these potential uncertainties in measurements, sediment transport model performance was considered to be reasonable.

3.4. Design Storm Application

The calibrated model was applied to design storm rainfall to simulate runoff and sediment transport that would occur for a very large storm event. As specified by Myongji University,

Table 9.4
Summary statistics for hydrologic model performance

Event	Station	Metric										
		Total flow volume (m^3)			Peak flow (m^3/s)			Time to peak flow (h)			Flow time series	
		Measured	Simulated	RPD (%)	Measured	Simulated	RPD (%)	Measured	Simulated	RPD (%)	NSEC	RMSE (%)
July 24–26, 2008	Hyangseok	8.21E + 07	9.09E + 07	10.72	1,619	1,615	−0.25	42.0	42.8	1.79	0.94	25.0
	Miho	8.45E + 07	8.36E + 07	−1.07	1,569	1,457	−7.14	34.0	41.9	23.09	0.62	61.6
	Wolho	3.27E + 07	3.11E + 07	−4.89	638	617	−3.30	30.0	34.8	16.00	0.84	38.0
	Yecheon	4.69E + 06	9.29E + 06	98.08	92	270	193.85	36.0	36.5	1.25	−4.47	199.2
July 8–10, 2009	Hyangseok	3.56E + 07	4.07E + 07	14.33	520	582	11.79	54.0	53.4	−1.11	0.80	42.5
	Miho	2.93E + 07	3.58E + 07	22.18	452	519	14.76	50.0	51.5	2.90	0.93	26.4
	Wolho	9.23E + 06	1.38E + 07	49.51	196	250	27.59	45.0	46.1	2.33	0.43	71.9
	Yecheon	4.35E + 06	7.25E + 06	66.67	90	188	107.45	44.0	43.7	−0.79	−1.02	133.6

Notes: (1) RPD = relative percent difference. RPD values were calculated as (Simulated − Measured)/Measured; (2) NSEC = Nash-Sutcliffe efficiency coefficient. NSCE values range from 1 to $-\infty$, with a value of 1 representing perfect agreement; (3) RMSE = root mean square error.

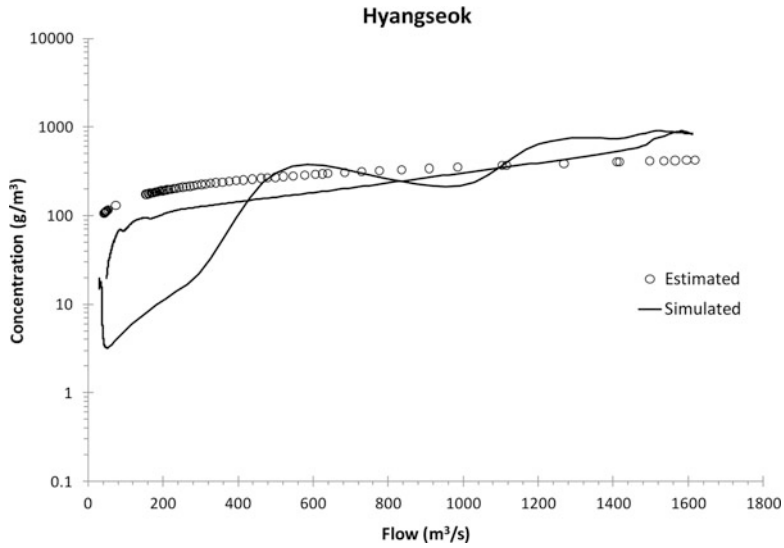

Fig. 9.6. Simulated and estimated total suspended solids concentrations at Hyangseok: July 24–26, 2008, storm.

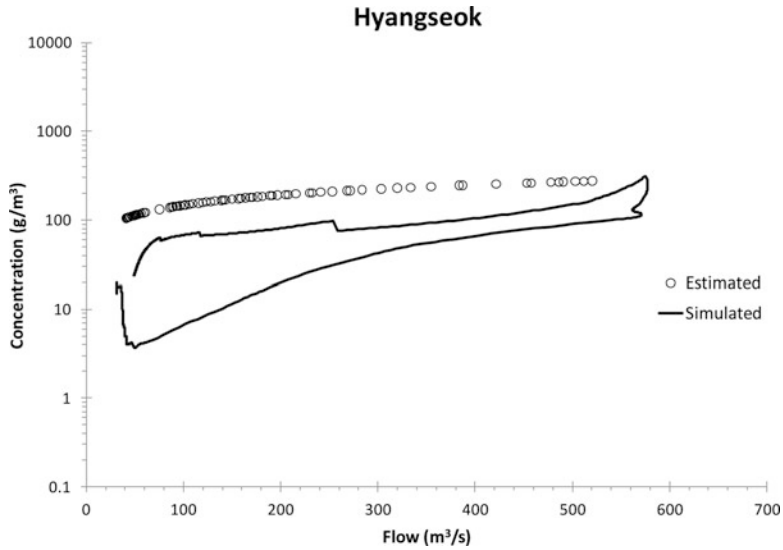

Fig. 9.7. Simulated and estimated total suspended solids concentrations at Hyangseok: July 8–10, 2009, storm.

this design storm delivers 300 mm of rain that is uniformly distributed over the entire watershed and which falls at a rate of 50 mm/h for 6 h. Initial moisture and water conditions for the design storm were assumed to be the same as those that occurred for the July 2009 rainfall event.

Table 9.5
Summary of measured, estimated, and simulated suspended solids concentrations

Station	Measured (g/m^3)		Estimated (g/m^3)		Simulated (g/m^3)		Storm
	Geometric mean	Range	Geometric mean	Range	Geometric mean	Range	
Hyangseok	30	7–210	187	106–423	48	3–901	July 2008
			159	105–275	31	4–308	July 2009
Gopyeong Bridge	15	6–30			63	5–1,040	July 2008
					43	7–326	July 2009
Songriwon	6	0.4–52	797	290–21,700	40	0.7–1,940	July 2008
			11	0.05–1,720	17	0.5–250	July 2009
Seokpo	4	0.4–22			4	5–1,950	July 2008
					4	3–260	July 2009

Notes: (1) Measured values were determined from samples collected at six stations within the watershed as part of monthly monitoring efforts during the month of July in 2003, 2006, 2008, and 2009 as detailed in the Myongji University database. For Hyangseok, the Naesung Stream 3, 3-1, and 3A stations were used to determine measured concentrations. For Gopyeong Bridge, the Naesung Stream 1 station was used. For Songriwon, the Yeongjuseo Stream 2 station was used. For Seokpo, the Naesung Stream 4 station was used; (2) estimated values were determined from flow and sediment-discharge relationships for each station.

Table 9.6
Summary of reported, estimated, and simulated sediment yield rates

Station	Drainage area (km^2)	Sediment yield rate (metric tons/km^2/year)		
		Reported	Estimated	Simulated
Hyangseok	1,630 (estimated)		660–2,100	345–3,110
Gopyeong Bridge	1,153	320		355–3,880
Songriwon Bridge	491	453	1,100–67,000	451–5,970
Seokpo Bridge	299	501		637–3,030
Bongwha	157	624		502–13,830

Notes: (1) Reported values were obtained from the Myongji University database; (2) estimated values were determined by calculating computing sediment loads using reported flows and sediment-discharge relationships where available; (3) simulated values for the July 2008 storm represent high values for the tabulated ranges. Simulated values for the July 2009 storm represent low values for tabulated ranges.

Visualizations of water depth and total suspended solids at Naesung Stream are presented in Figs. 9.8 and 9.9. Surface runoff in the main channel can be observed at 4 h and is dominant at 8 h after the beginning of the storm. Upland erosion losses are clearly visible from the mountain areas 4 h after the beginning of the storm. High sediment concentrations then reach the valleys after 8 h and sediment settling takes place after 8 h.

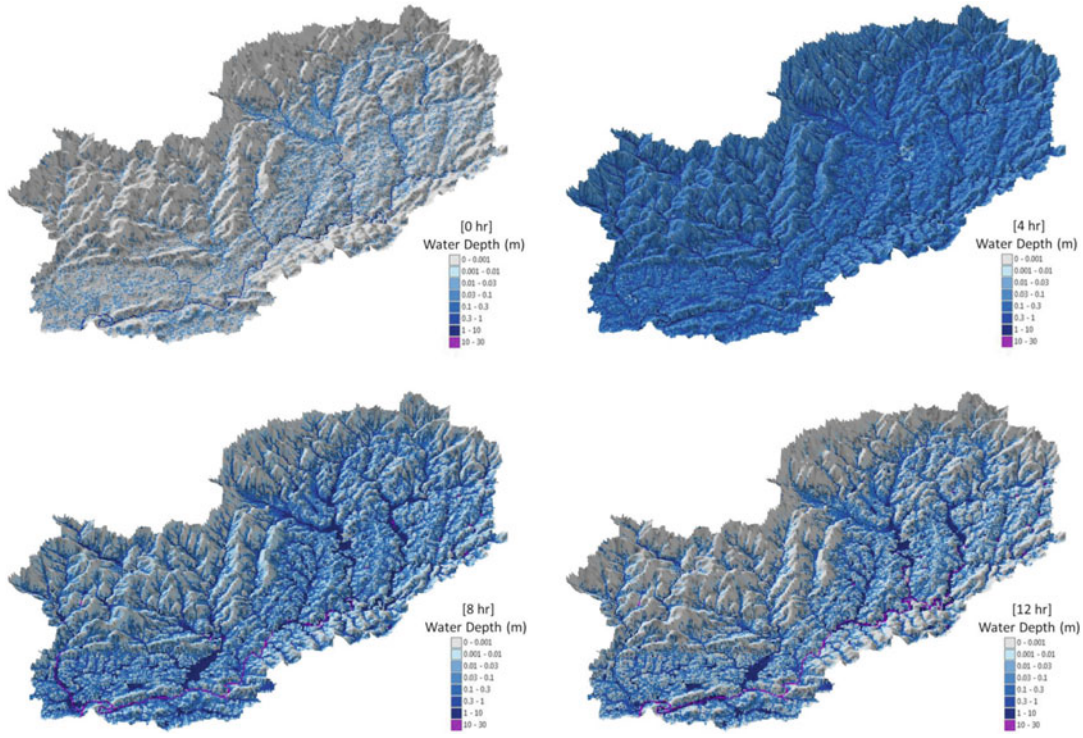

Fig. 9.8. Visualization of Naesung Stream design storm water depths: 0, 4, 8, and 12 h after storm starts.

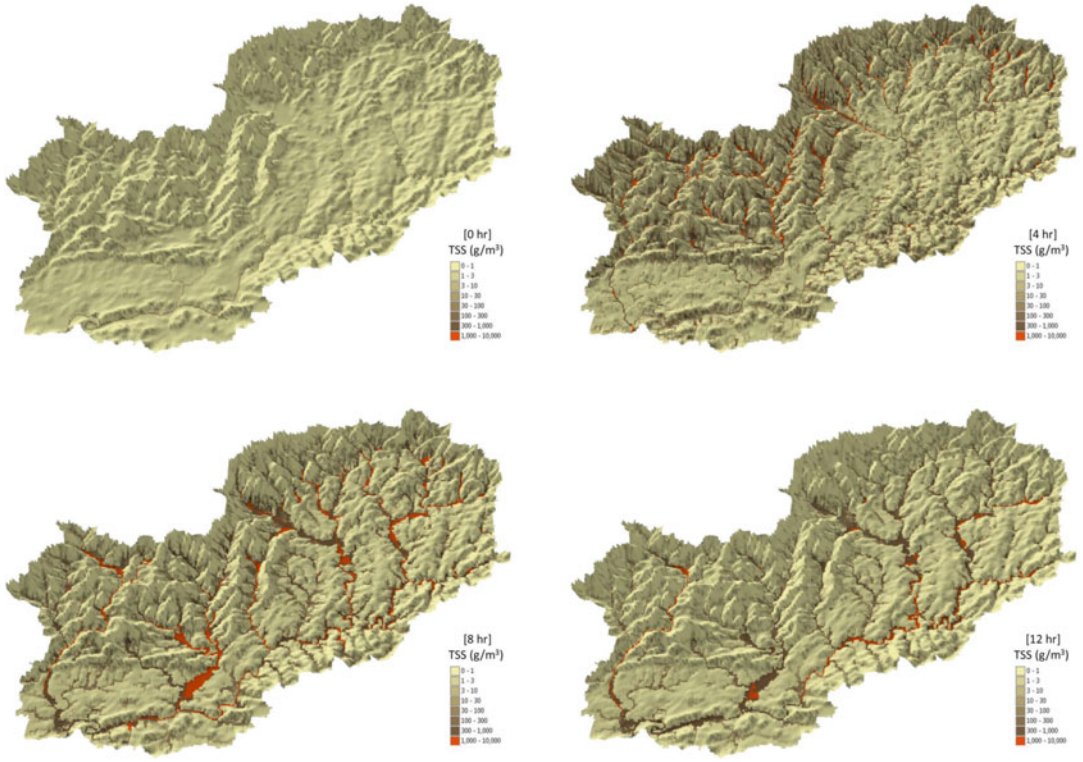

Fig. 9.9. Visualization of Naesung Stream design storm total suspended solids (TSS): 0, 4, 8, and 12 h after storm starts.

ACKNOWLEDGEMENTS

The TREX model development has been developed by P. Julien's research group at Colorado State University, with funding from the Center for Geosciences/Atmospheric Research under Cooperative Agreement DAAD19-02-2-0005. The application at Naesung Stream has been the result of collaboration between HDR|HydroQual, Colorado State University, and Myongji University. These applications were supported by a grant for the project "Sediment Management Plan Development for Channel Stabilization" from K-Water (Korea Water Resources Corporation) funded by Ministry of Land, Transport and Maritime Affairs of the Korean government. We are grateful to Masatsugu (Masa) Takamatsu, Lihong (Lucy) Yang, Daniel Schwartz, Christopher Fanelli, and James Hallden at HDR|HydroQual and Jazuri Abdullah, James Halgren, and Andy Steininger at Colorado State University and Eunkyung Jang at Myongji University.

REFERENCES

1. Green WH, Ampt GA (1911) Studies on soil physics. 1: The flow of air and water through soils. J Agric Sci 4(1):11–24
2. Richards LA (1931) Capillary conduction of liquids in porous mediums. Physics 1:318–333
3. Philip JR (1957) The theory of infiltration: 1. The infiltration equation and its solution. Soil Sci 83:345–357
4. Smith RE, Parlange J-Y (1978) A parameter efficient hydrologic infiltrations model. Water Resour Res 14(3):533–538
5. Julien PY, Saghafian B, Ogden FL (1995) Raster-based hydrologic modeling of spatially-varied surface runoff. J Am Water Resour Assoc 31(3):523–536
6. Julien PY (2002) River mechanics. Cambridge University Press, Cambridge, UK, p 434
7. Julien PY, Simons DB (1985) Sediment transport capacity of overland flow. Trans Am Soc Agric Eng 28(3):755–762
8. Julien PY, Frenette M (1985) Modeling of rainfall erosion. J Hydraul Eng 11(10):1344–1359
9. Aksoy H, Kavvas ML (2005) A review of hillslope and watershed scale erosion and sediment transport models. Catena 64(2–3):247–271
10. Merritt WS, Letcher RA, Jakeman AJ (2003) A review of erosion and sediment transport models. Environ Model Softw 18(8–9):761–799
11. Wischmeier WH, Smith DD (1978) Predicting soil erosion losses: a guide to conservation planning, vol 537, Agricultural handbook. U.S. Department of Agriculture, Washington, DC, p 58
12. Renard KG, Foster GR, Weesies GA, Porter JP (1991) RUSLE: revised universal soil loss equation. J Soil Water Conserv 46(1):30–33
13. Renard KG, Foster GR, Yoder DC, McCool DK (1994) RUSLE revisited: status, questions, answers, and the future. J Soil Water Conserv 49(3):213–220
14. Renard KG, Foster GR, Weesies GA, McCool DK, Yoder DC (1997) Predicting soil erosion by water: a guide to conservation planning with the revised universal soil loss equation (RUSLE), vol 703, Agricultural handbook. U.S. Department of Agriculture, Washington, DC, p 407
15. Foster GR, Toy TE, Renard KG (2003) Comparison of the USLE, RUSLE1.06 and RUSLE2 for application to highly disturbed lands. In: Renard KG, McIlroy SA, Gburek WJ, Cranfield HE,

Scott RL (eds) First interagency conference on research in watersheds. U.S. Department of Agriculture, Washington, DC
16. Williams JR (1975) Sediment routing for agricultural watersheds. Water Resour Bull 11(5):965–974
17. Kinnell PIA (2010) Event soil loss, runoff and the Universal Soil Loss Equation family of models: a review. J Hydrol 385(1–4):384–397
18. Prosser IP, Rustomji P (2000) Sediment transport capacity relations for overland flow. Prog Phys Geogr 24(2):179–193
19. Julien PY (2010) Erosion and sedimentation, 2nd edn. Cambridge University Press, Cambridge, UK, p 371
20. Kilinc MY, Richardson EV (1973) Mechanics of soil erosion from overland flow generated by simulated rainfall, vol 63, Hydrology papers. Colorado State University, Fort Collins, CO
21. Meyer LD, Wischmeier WH (1969) Mathematical simulation of the process of soil erosion by water. Trans Am Soc Agric Eng 12(6):754–762
22. Yang CT (1996) Sediment transport: theory and practice. McGraw-Hill Inc., New York, p 396
23. Engelund F, Hansen E (1967) A monograph on sediment transport in alluvial streams. Teknisk Vorlag, Copenhagen, Denmark, p 62
24. Cheng NS (1997) Simplified settling velocity formula for sediment particle. J Hydraul Eng 123(2):149–152
25. Burban PY, Xu Y, McNeil J, Lick W (1990) Settling speeds of flocs in fresh and sea waters. J Geophys Res C Oceans 95(C10):18213–18220
26. Krishnappan BG (2000) In situ distribution of suspended particles in the Frasier River. J Hydraul Eng 126(8):561–569
27. Haralampides K, McCorquodale JA, Krishnappan BG (2003) Deposition properties of fine sediment. J Hydraul Eng 129(3):230–234
28. Krone RB (1962) Flume studies of the transport of sediments in estuarial shoaling processes. Final Report, Hydraulic Engineering Laboratory and Sanitary Engineering Research Laboratory, University of California, Berkeley, California
29. Beuselinck L, Govers G, Steegen A, Quine TA (1999) Sediment transport by overland flow over an area of net deposition. Hydrol Process 13(17):2769–2782
30. Mehta A, McAnally W, Hayter E, Teeter A, Heltzel S, Carey W (1989) Cohesive sediment transport. II: Application. J Hydraul Eng 115(8):1094–1112
31. Singh VP (1995) Computer models of watershed hydrology. Water Resources Publications, Highlands Ranch, CO, p 1144
32. Julien PY, Saghafian B (1991) CASC2D user's manual—A two dimensional watershed rainfall-runoff model. Report CER90-91PYJ-BS-12. Department of Civil Engineering, Colorado State University, Fort Collins, Colorado, p 66
33. Johnson BE, Julien PY, Molnar DK, Watson CC (2000) The two-dimensional upland erosion model CASC2D-SED. J Am Water Resour Assoc 36(1):31–42
34. Ogden FL, Julien PY (2002) CASC2D: a two-dimensional, physically-based, hortonian hydrologic model. In: Singh VP, Frevert D (eds) Mathematical models of small watershed hydrology and applications. Water Resources Publications, Littleton, CO, pp 69–112
35. Julien PY, Rojas R (2002) Upland erosion modeling with CASC2D-SED. Int J Sediment Res 17(4):265–274
36. Downer CW, Ogden FL (2004) GSSHA: model to simulate diverse stream flow producing processes. J Hydrol Eng 9(3):161–174

37. Abbott MB, Bathurst JC, Cunge JA, O'Connell PE, Rasmussen J (1986) An introduction to the European Hydrological System—Système Hydrologique Europèen, SHE.1: History and philosophy of a physically-based, distributed modelling system. J Hydrol 87(1–2):45–59
38. Wicks JM, Bathurst JC (1996) SHESED: a physically based, distributed erosion and sediment yield component for the SHE hydrological modeling system. J Hydrol 175(1–4):213–238
39. Ewen J, Parkin G, O'Connell PE (2000) SHETRAN: distributed river basin flow and transport modeling system. J Hydrol Eng 5(3):250–258
40. Abbott MB, Bathurst JC, Cunge JA, O'Connell PE, Rasmussen J (1986) An introduction to the European Hydrological System—Système Hydrologique Europèen, SHE. 2: Structure of a physically-based, distributed modelling system. J Hydrol 87(1–2):61–77
41. Velleux M, England J, Julien P (2008) TREX: spatially distributed model to assess watershed contaminant transport and fate. Sci Total Environ 404(1):113–128
42. England J, Velleux M, Julien P (2007) Two-dimensional simulations of extreme floods on a large watershed. J Hydrol 347(1):229–241
43. Velleux M (2005) Spatially distributed model to assess watershed contaminant transport and fate. Ph.D. dissertation, Department of Civil Engineering, Colorado State University, Fort Collins, Colorado, p 261
44. Rojas R (2002) GIS-based upland erosion modeling, geovisualization and grid size effects on erosion simulations with CASC2D-SED. Ph.D. dissertation, Department of Civil Engineering, Colorado State University, Fort Collins, Colorado
45. Molnár DK, Julien PY (2000) Grid size effects on surface runoff modeling. J Hydrol Eng 5(1):8–16
46. Velleux M, Julien P, Rojas-Sanchez R, Clements W, England J (2006) Simulation of metals transport and toxicity at a mine-impacted watershed: California Gulch, Colorado. Environ Sci Technol 40(22):6996–7004
47. Ambrose RB, Martin JL, Wool TA (1993) WASP5, a hydrodynamic and water quality model—model theory, user's manual, and programmer's guide. U.S. Environmental Protection Agency, Office of Research and Development, Environmental Research Laboratory, Athens, GA
48. Velleux M, Westenbroek S, Ruppel J, Settles M, Endicott D (2001) A user's guide to IPX, the in-place pollutant export water quality modeling framework, Ver. 2.7.4. EPA/600/R-01/079. U.S. Environmental Protection Agency, Office of Research and Development, National Health and Environmental Effects Research Laboratory, Mid-Continent Ecology Division, Large Lakes Research Station, Grosse Ile, Michigan, p 179
49. MJU (2010) Naesung stream watershed data collection. Prepared by Myongji University, Yongin, South Korea
50. MJU (2011) Naesung stream watershed bank erosion. Prepared by Myongji University, Yongin, South Korea
51. ESRI (2008) ArcGIS 9.3. Environmental Systems Research Institute, Redlands, CA
52. USACE (2008) HEC-RAS, river analysis system user's manual, version 4.0. U.S. Army Corps of Engineers, Hydrologic Engineering Center (HEC), Davis, CA
53. Rojas R, Velleux M, Julien P, Johnson B (2008) Grid scale effects on watershed soil erosion models. J Hydrol Eng 13(9):793–802
54. Tarboton D (1997) A new method for the determination of flow directions and upslope areas in grid digital elevation models. Water Resour Res 33(2):309–319

55. Jia Y, Kinouchi T, Yoshitani J (2005) Distributed hydrologic modeling in a partially urbanized agricultural watershed using water and energy transfer process model. J Hydrol Eng 10(4):253–263
56. Linsley RK, Kohler MA, Paulhus JLH (1982) Hydrology for engineers, 3rd edn. McGraw-Hill Book Company, New York, p 508
57. Woolhiser DA, Smith RE, Goodrich DC (1990) KINEROS, a kinematic runoff and erosion model: documentation and user manual. U.S. Department of Agriculture, Agriculture Research Service, ARS-77, Mar 1990
58. Bras RL (1990) Hydrology: an introduction to hydrologic science. Addison-Wesley Publishing Company, Reading, MA, p 643
59. USACE (1998) HEC-1 flood hydrograph package user's manual. Report: CPD-1A. U.S. Army Corps of Engineers, Hydraulic Engineering Center, Davis, CA, June 1998
60. Chow VT (1959) Open-channel hydraulics. McGraw-Hill, New York, p 680, Reissued 1988
61. Rawls WJ, Ahuja LR, Brakensiek DL, Shirmohammadi A (1993) Infiltration and soil movement. In: Maidment DR (ed) Handbook of hydrology. McGraw-Hill, Inc., New York, pp 5.1–5.51